Clays and Clay Minerals, Vol. 58, No. 4, 558–572, 2010.

FACTORS CONTROLLING THE EVOLUTION OF MINERAL ASSEMBLAGES AND ILLITE CRYSTALLINITY IN PALEOZOIC TO TRIASSIC SEQUENCES FROM THE TRANSITION BETWEEN MALÁGUIDE AND ALPUJÁRRIDE COMPLEXES (BETIC CORDILLERA, SPAIN): THE SIGNIFICANCE OF TOBELITE

M. D. Ruiz Cruz[1,*] and C. Sanz de Galdeano[2]

[1] Departamento de Química Inorgánica, Cristalografía y Mineralogía, Facultad de Ciencias, Universidad de Málaga, 29071 Málaga, Spain

[2] Instituto Andaluz de Ciencias de la Tierra, CSIC-Universidad de Granada, Facultad de Ciencias, 18071-Granada, Spain

Abstract—The Hercynian metamorphic event is poorly characterized in internal zone complexes of the Betic Cordillera (Spain), as it has been, to a great extent, overprinted by the mineral assemblages formed during the Alpine event. Identification of the signals of the Hercynian episode is easier in series largely unaffected by the Alpine event, such as Intermediate units between the Maláguide and the Alpujárride Complexes, which consist of a set of thrust slices. With the aim of characterizing the Hercynian paragenesis, a detailed comparison of the mineral assemblages of Paleozoic and overlying Triassic sequences, unaffected by the pre-Alpine event, was carried out. Mineral assemblages were characterized by X-ray diffraction, infrared spectroscopy, scanning electron microscopy, electron microprobe, and transmission-analytical electron microscopy. A rapid increase in the illite crystallinity values was observed at the Triassic–Paleozoic transition in the upper tectonic slices. In addition, the diagenetic to anchizonal dickite-, sudoite-, and pyrophyllite-bearing assemblages, characterizing the Triassic rocks, contrast with Paleozoic assemblages consisting of white K-mica ± paragonite + chlorite + mica-chlorite and chlorite-vermiculite mixed layers + garnet, suggesting that this assemblage corresponds to the Hercynian metamorphic event. This assemblage records temperatures on the order of 400ºC and an intermediate pressure regime. Paleozoic rocks contain, in addition, tobelite, which comprises some of the detrital grains and strongly masks the illite crystallinity values. Tobelite has been identified only in the upper thrust slices, suggesting that changes in the detrital input is primarily responsible for the disappearance of tobelite at the transition from the Maláguide to the Alpujárride domain. Tobelite appears finely intergrown with white K-mica and its origin is uncertain. It could have been inherited as tobelite, but a more likely hypothesis is that the intergrowths of white K-mica and tobelite were formed at low temperature from an NH_4-bearing mica precursor.

Key Words—Alpine Metamorphism, Alpujárride Complex, Betic Cordillera, Hercynian Metamorphism, Maláguide Complex, Tobelite, White K-mica.

INTRODUCTION

The Internal Zone of the Betic Cordillera, the westernmost European Alpine chain, consists of three superimposed tectonic complexes (Figure 1), which from bottom to top are: the Nevado-Filábride, the Alpujárride, and the Maláguide (Egeler and Simon, 1969). The geotectonic relations between the Maláguide and the Alpujárride are essentially constant in the Betic Cordillera: the Maláguide complex tectonically overlies the Alpujárride complex. Generally, Maláguide and Alpujárride Triassic units are easily distinguished on the basis of their different lithologies and metamorphic grade. Nevertheless, transitional zones with intermediate lithologies and metamorphism have been identified in several areas of the Cordillera and are known as "intermediate units" (Paquet, 1969; Mäkel and Rondeel, 1979; Sanz de Galdeano *et al*., 2001).

The existence of a Hercynian event has been proved in Maláguide terranes (less affected by the Alpine event), on the basis of the rapid increase in the mica and chlorite crystallinity in Paleozoic units relative to the overlying Triassic terranes (Felder, 1980; Mäkel, 1985; Ruiz Cruz, 1997). In contrast, the metamorphism characterizing the Alpujárride Paleozoic units has been interpreted as Alpine, though the existence of a Hercynian event has also been demonstrated on the basis of the zircon ages (Zeck and Whitehouse, 1999). Intermediate units between Maláguide and Alpujárride complexes seem to be appropriate for studying the change in metamorphic conditions at the transition from typical Maláguide to typical Alpujárride terranes.

In very low- and low-grade metaclastic rocks, such as those studied here, diagnostic metamorphic minerals are generally lacking and the determination of metamorphic grade must be based on the study of the clay mineral associations, as observed by X-ray diffraction (XRD).

* E-mail address of corresponding author:
mdruiz@uma.es
DOI: 10.1346/CCMN.2010.0580410

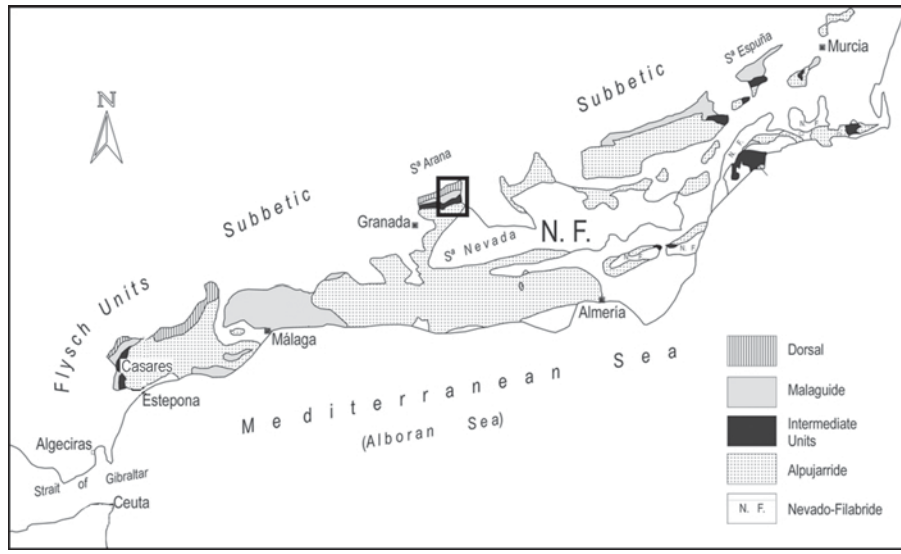

Figure 1. Tectonic map of the Betic Cordillera and location of the zone studied (modified from Sanz de Galdeano *et al*., 2001).

The classical methods include the determination of the illite and chlorite crystallinity and the white K-mica *b* cell dimension (Merriman and Peacor, 1999). In most recent years, transmission electron microscopy (TEM) has also been used in the characterization of rocks subject to diagenesis and low-grade metamorphism. Using TEM techniques, Merriman *et al.* (1990, 1995) showed that the width of the 10 Å peak is largely controlled by the thickness of illite-muscovite crystallites, although lattice strain also influences the 10 Å peak width (Árkai *et al*., 1996). In addition, other factors are known to influence illite-muscovite peak shape, particularly the interference from other phyllosilicates (Frey, 1987; Árkai *et al*., 2004) and especially the presence of Na- and NH_4-bearing micas, which can cause a notable broadening of the 10 Å peak, leading to erroneous Kübler index (KI) values. Detection of the presence of NH_4-bearing mica is difficult, especially if the NH_4-content in white K-mica is small. The presence of detrital input in the <2-μm size fractions is another factor of uncertainty. The <2-μm size fractions are generally assumed to contain authigenic minerals. Nevertheless, the presence of fine-grained detrital particles cannot be discarded on the basis of the XRD data. In this case, the validity of the KI values is also questionable.

The NH_4-analog of muscovite (tobelite) has been described as being predominantly associated with two different geologic settings: (1) diagenetic to low-grade metamorphic shales from meta-anthracite and anthracite coalfields (*e.g.* Juster *et al*., 1987; Daniels and Altaner, 1990; Wilson *et al.*, 1992; Ward and Christie, 1994; Liu *et al*., 1996); and (2) hydrothermal deposits or hydrothermally altered areas (*e.g.* Higashi, 1982; Bobos and Ghegary, 1999). The origin of the dioctahedral NH_4-mica is uncertain. In coal-associated shales, NH_4-mica is generally interpreted as having formed from reaction of kaolinite, smectite, or K-mica with NH_3 expelled from coal seams. Dioctahedral NH_4-mica has also been described in anchizonal samples, where neither coal seams nor hydrothermal activity are evident (Árkai *et al.*, 2004). A possible detrital origin for tobelite has not been reported previously.

The focus of the present study was on the evolution of the clay mineral associations at the transition from Paleozoic to Triassic sequences in units transitional between the Maláguide and the Alpujárride complexes from the central zone of the Cordillera. Most of the data on the mineralogy of the Triassic sequences have been published previously (*e.g.* Ruiz Cruz *et al.*, 2005), and will be used here for comparison. The mineral evolution observed in both the transition from Paleozoic to Triassic and from Maláguide- to Alpujárride-like units can be influenced by metamorphic grade, by variations in the paleogeographic position, and by the nature of the detrital supplies. These factors were analyzed starting from the evolution of clay mineral assemblages, from the crystal-chemical parameters of white K-mica, and from the presence of other, scarcer metamorphic phases. Special attention was devoted to the characterization and significance of tobelite, which had not been described previously in these units.

GEOLOGIC SETTING AND SAMPLING

Both the Alpujárride and the Maláguide complexes include Triassic and Paleozoic sequences. Though the metamorphic patterns of the Triassic terranes have been well studied in both complexes, interpretation of the Paleozoic assemblages is difficult because the Alpine

metamorphic event has locally overprinted the older metamorphic assemblages, especially in the case of the Alpujárride complex.

The Alpujárride complex shows sequences consisting of Paleozoic to Triassic rocks. The Triassic rocks are characterized by the presence of blue phyllites, blue-to-white schists, and calc-schists, quartzites, and marbles. The Paleozoic rocks are mainly greywackes and schists, which evolve with depth toward gneisses or even migmatites. Triassic rocks show an Alpine low-temperature-high-pressure (L*T*-H*P*) metamorphism, overprinted by a high-temperature-low-pressure (H*T*-L*P*) one (Azañón *et al.*, 1998; Goffé et al., 1989; Booth-Rea *et al*., 2002).

The Maláguide complex includes sediments from Paleozoic to Tertiary ages. The Triassic sequences, characterized by the presence of red conglomerates, red sandstones, red lutites, and minor carbonates, show a transition from low diagenesis to anchizone (Ruiz Cruz and Rodríguez Jiménez, 2002). The Paleozoic sequences mainly consist of blue phyllites (Ordovician-Silurian), limestones (Devonian), and a greywacke-shale alternation (Devonian-Carboniferous). Discontinuous levels of conglomerates ('Marbella conglomerates') appear in the upper part of the Paleozoic sequence.

In the intermediate units, the Triassic rocks from the upper thrust slices (Figure 2) show lithologic characteristics and metamorphic patterns similar to those of the Maláguide complex (with typical red color), whereas increase in depth is characterized by the presence of intermediate lithologies and metamorphic patterns, and later by lithologies and mineral assemblages more like those of the Alpujárride complex (with typical blue colors). In contrast, Paleozoic rocks show homogeneous lithologies (greywackes, shales, and calc-schists) through the tectonic pile, in most cases similar to Carboniferous sequences from the Maláguide complex. The intermediate units are suitable zones for studying the evolution of the mineral associations at the Paleozoic to Triassic transition and at the transition from Maláguide- to Alpujárride-like slices, as the presence of numerous thinned thrust slices favors the identification of the mineral evolution in relatively restricted areas.

The Paleozoic rocks were sampled in the central (Sierra Arana) and western zones (Casares) of the Betic Cordillera (Figure 1), although the results shown here are limited to the central zone. At the Sierra Arana area, sampling was carried out in two sectors (Diezma and El Molinillo) (Figure 2). Several superimposed thrust slices varying in thickness from 50 to 300 m are present in this area. A total of 78 samples was taken.

METHODOLOGY

Samples were studied systematically by X-ray diffraction (XRD). Petrographic microscopy was used in samples with appropriate grain size. Scanning electron microscopy (SEM) or electron microprobe analysis (EMPA) was used in selected samples, depending on the grain size. Samples were also investigated by transmission-analytical electron microscopy (TEM-AEM) and infrared spectroscopy (IR).

The XRD patterns were recorded using a Siemens D-5000 diffractometer (Málaga University) with CuKα radiation and a graphite monochromator, operated at 40 mA and 40 kV, with a 0.01º2θ step size and 2 s counting time. Randomly oriented samples were used for determination of the *b* parameter of the phyllosilicates (<2 μm size fractions). Oriented samples, prepared in the air-dried state (natural and Mg-saturated) after ethylene-glycol solvation and after heating at 550ºC were used for phyllosilicate identification. The Kübler index (Kübler, 1968) was measured in fine-grained samples, following the recommendations of Kisch (1991). The KI measurements (x) were transformed into Crystallinity Index Standards (CIS) values (y, Warr and Rice, 1994) according to the equation $y = 1.23x - 0.07$. Deconvolution of the mica peaks was carried out using the *Peakfit* software from Jandel Scientific (San Rafael, USA). Peak fitting was carried out using a Pearson IV function with the minimum number of components until correlation coefficients with $r^2 > 0.997$ were obtained.

Polished and carbon-coated thin sections were analyzed by EMPA, using a Cameca model SX-50 instrument (CIC, Granada University). ZAF (atomic number, absorption, and fluorescence) corrections and data reductions were performed with the software package supplied by Cameca. The accelerating voltage was 20 kV and the probe current was 20 nA. Standards were wollastonite (Si and Ca), synthetic Al_2O_3 (Al), orthoclase (K), albite (Na), synthetic Fe_2O_3 (Fe), periclase (Mg), and synthetic $MnTiO_3$ (Mn and Ti). Thin sections were also studied by SEM, using a ZEISS DSM 950 scanning electron microscope equipped with an X-ray energy dispersive (EDX) system (LINK QX 2000) at an accelerating voltage of 14 kV and 2 nA probe current (CIC, University of Granada). The standards used were albite (Na), orthoclase (K), periclase (Mg), wollastonite (Si, Ca), and synthetic oxides (Al_2O_3, Fe_2O_3, and $MnTiO_3$).

A set of selected areas was ion thinned for the TEM-AEM study. This study was also performed at the Granada University (CIC), with a 200 kV Philips CM-20 transmission electron microscope, fitted with a scanning transmission (STEM) device and solid state detector for energy-dispersive analysis. Microanalyses were obtained in STEM mode. Quantitative determinations used the thin-film approximation of Cliff and Lorimer (1975). Albite (Na and Al), muscovite (K and Al), annite (K, Mg and Fe), spessartine (Al and Mn), forsterite (Mg and Fe), and titanite (Ca and Ti) were used as standards.

The Fourier-transform infrared (FTIR) spectra were recorded from KBr pellets (2 wt.% samples) using a

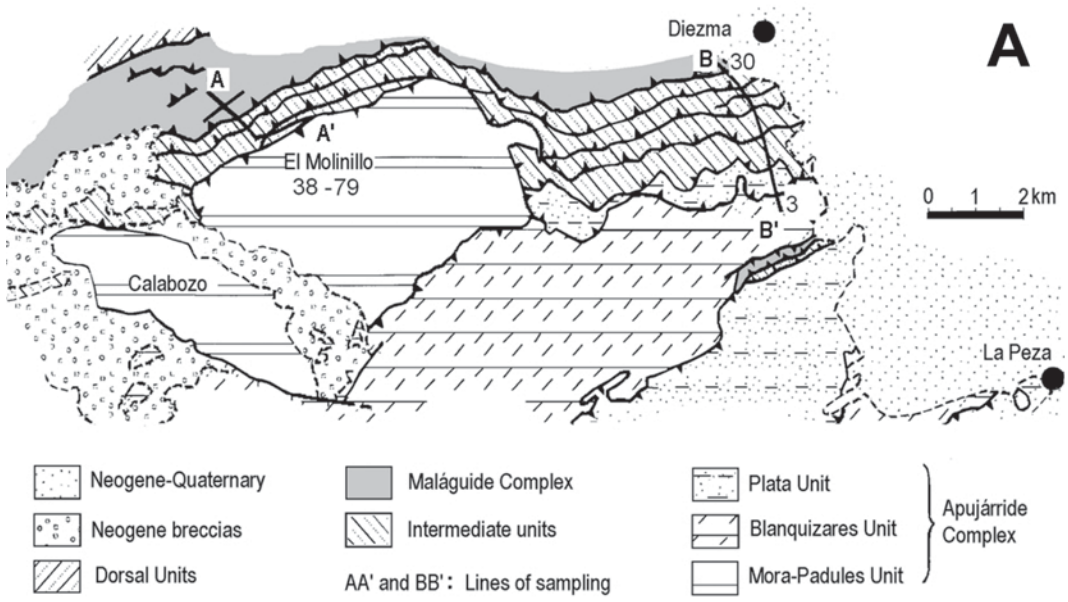

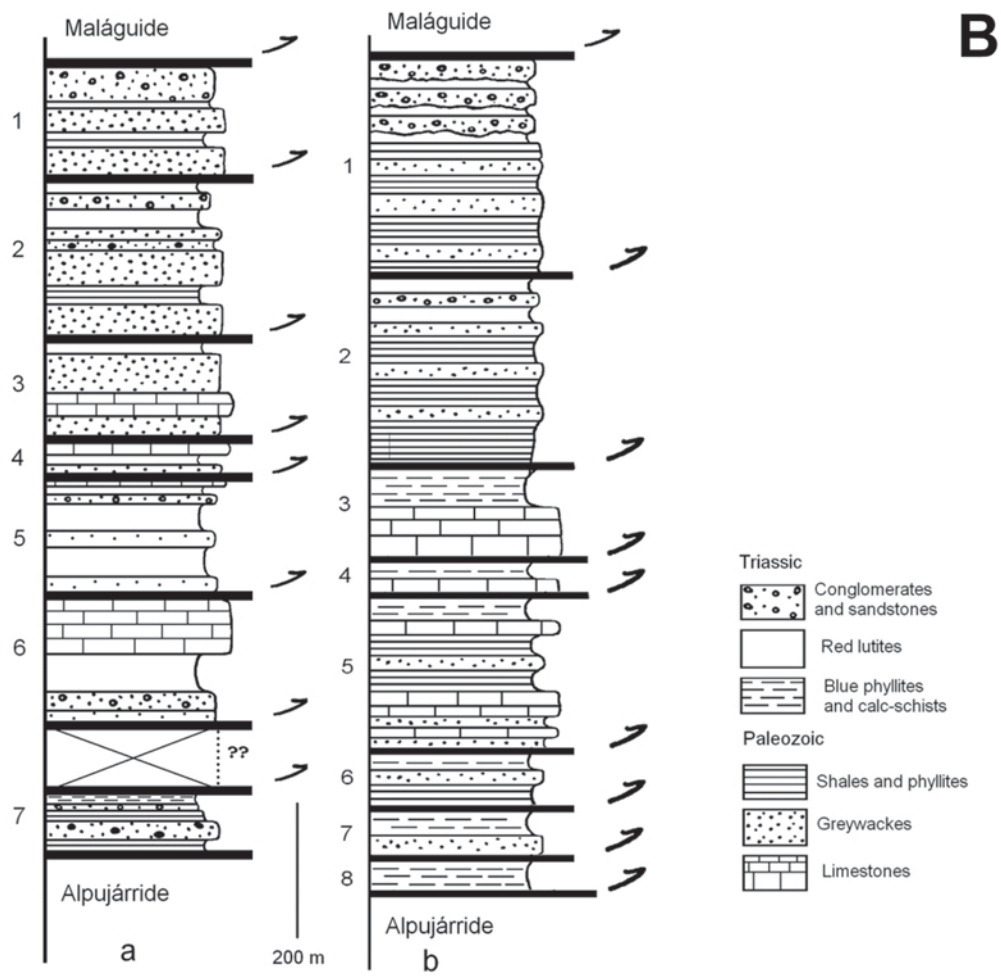

Figure 2. (A) Schematic map of the sampling area and location of the sections. AA': El Molinillo section. BB': Diezma section. (B) Lithologic columns of both sections: (a) El Molinillo column; (b) Diezma column (modified from Ruiz Cruz *et al.*, 2005).

Nicolet spectrometer (20SXB) with a DTGS detector, over the range 4000−400 cm^{-1} (Málaga University) with a resolution of 2 cm^{-1}. 300 scans were accumulated to improve the signal-to-noise ratio in the spectra. To avoid grinding effects in the preparation of the disks, the samples and KBr were gently mixed manually.

The mineral symbols of Kretz (1983) were used except for Dk: dickite, Tob: tobelite, Sud: sudoite, and ML: mixed layers. Ms includes muscovite (or phengite) and illite.

PETROGRAPHY

The Triassic samples studied by petrographic microscopy included conglomerates and sandstones from upper slices and phyllites from deeper slices. A detailed description can be found in Ruiz Cruz *et al.* (2005). In coarse-grained rocks, authigenic minerals are mainly found filling the secondary porosity. Dickite, dominant in the uppermost slices, is gradually replaced by white mica, pyrophyllite, and sudoite at increasing tectonic grade (Figure 3a). Only phyllites from the deep slices show grain sizes appropriate for microscopic study. The phyllites show a well developed slaty cleavage defined by chlorite and white mica, with occasional chloritoid (Figure 3b).

Paleozoic samples studied by petrographic microscopy include 'Marbella conglomerates' and greywackes from all slices, and phyllites and calc-schists from the deeper slices. Conglomerates are scarce and show rather uniform characteristics; they display poor sorting and consist of well rounded grains of quartz, albite, and fragments of metamorphic rocks (mainly quartzite and phyllite). Long detrital mica grains are rare, but they contain a fine-grained matrix consisting of white mica and chlorite. Fe-oxide, zircon, and rutile are accessory constituents. Vermiculitized detrital biotite is also common in these rocks.

Greywackes show variable grain size and textural characteristics depending on their grain size and tectonic position, although the mineral association is rather uniform. A null to poorly marked schistosity characterizes the greywackes of the upper thrust slices. At increasing tectonic grade, greywackes show a progressively better developed schistosity parallel to bedding (Figure 3c). Greywackes consist of detrital grains of quartz, fragments of metamorphic rocks (mainly quartzite and phyllite), albite, muscovite, vermiculitized biotite, and chlorite. Rounded, chlorite-rich chlorite + muscovite stacks variably transformed into mixed-layer phases (regular 1:2 mica/chlorite, after Ruiz Cruz and Nieto, 2006) are also frequent detrital components

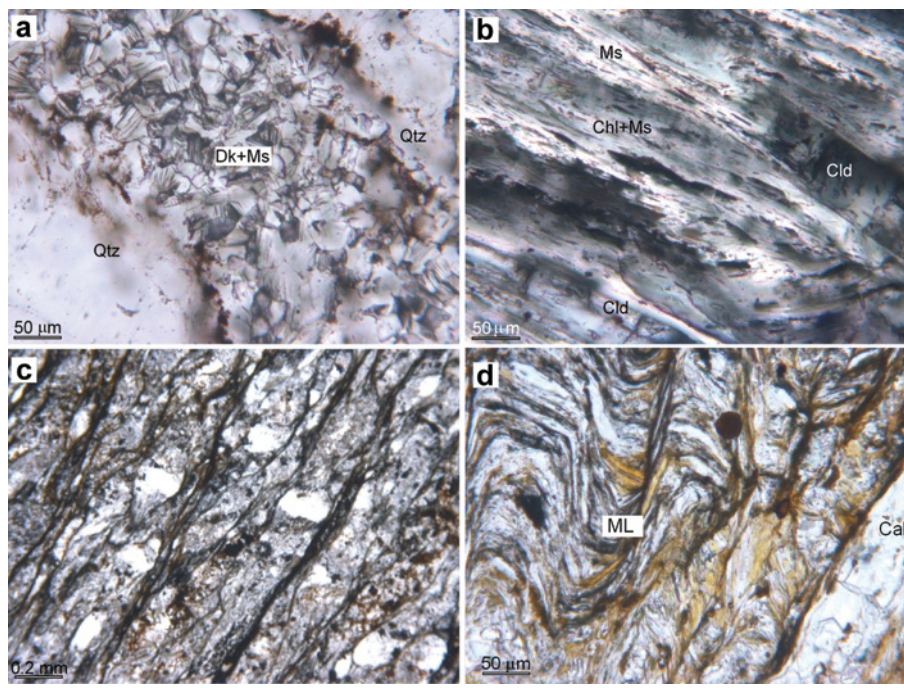

Figure 3. Photomicrographs showing textures in Triassic and Paleozoic rocks (plane-polarized light). (a) Dickite booklets partially transformed into illite, filling pores in a Triassic sandstone from the upper slices. (b) Prismatic crystals of chloritoid in Triassic blue phyllite from the lower slices. (c) Incipient schistosity, parallel to bedding in a Paleozoic greywacke from the lower slices. (d) Brownish laths of mixed layers following S_0 and S_1 in Paleozoic calc schist from the lower slices. Mineral symbols according to Kretz (1983) except for Dk: dickite. Ms includes muscovite (or phengite) and illite.

(Figure 4a,b). Only scarce muscovite, chlorite, and mixed layers, filling the pores or parallel to the schistosity, appear to be authigenic. Carbonates appear as small rhombs of calcite and minor dolomite, frequently rimmed by ankerite. Accessory minerals are zircon, tourmaline, rutile, and Fe oxide. Minute garnet grains, which grew in the interstices between the detrital grains, are occasional constituents of the greywackes (Figure 4c,d).

Phyllites and calc-schists show two identifiable schistosities; the first, S_0, coinciding with the bedding, is defined by bands rich in Fe- and Ti oxides associated with white mica, chlorite, and brownish phases, previously identified as chlorite-vermiculite mixed layers (Ruiz Cruz and Nieto, 2006). The second, S_1, schistosity is a slaty cleavage defined by flakes of white mica, chlorite, brownish flakes of mixed layers, and Fe oxides (Figure 3d).

XRD and IR results

Different clay mineral assemblages have been identified at increasing tectonic grade (transition from Maláguide- to Alpujárride-like domains) in Triassic and Paleozoic samples (Figure 5). Triassic samples from slice 1 (Diezma sector) or slices 1 and 2 (El Molinillo sector) are characterized by the association Ms + Dk, with sporadic occurrences of chlorite. The KI values range from 0.50 to 0.75 in pelitic rocks. In slices 2 (Diezma)−3 (El Molinillo) the clay mineral association is Ms + Prl ± Prg + Chl ± Sud. The KI values range from 0.39 to 0.74. From slices 4 (Diezma) and 5 (El Molinillo), typical red sandstones are rare, being replaced by purple and later by blue phyllites and quartzites. The clay mineral association is dominated by Ms + Chl, with sporadic paragonite, coexisting in the deepest slices with chloritoid. The KI ranges from 0.24 to 0.34.

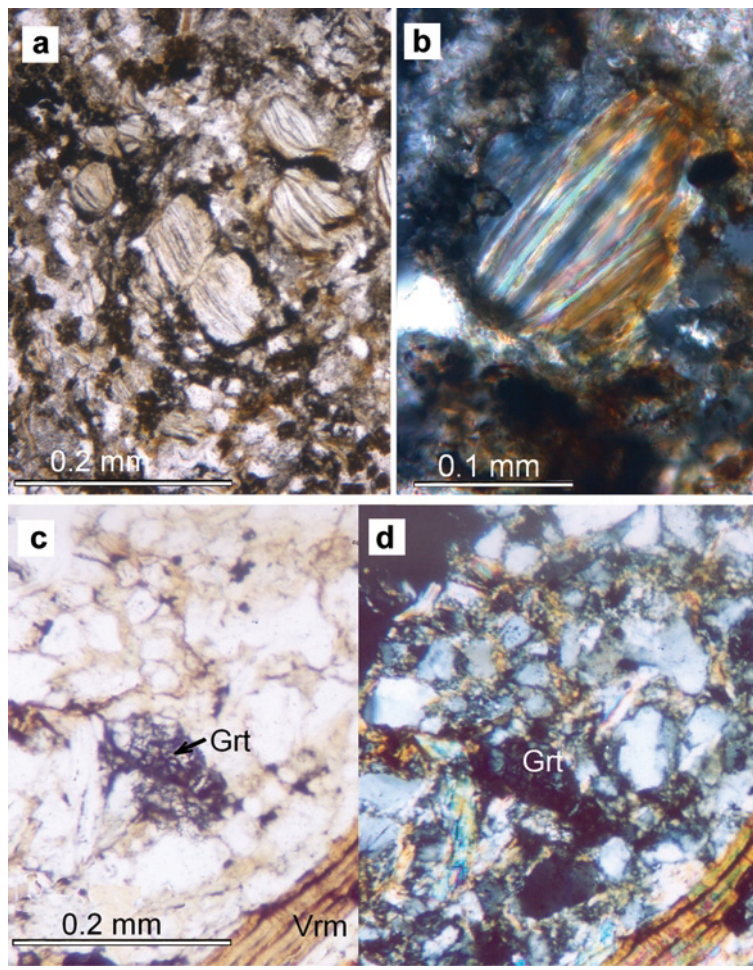

Figure 4. (a) Rounded, chlorite-rich detrital stacks in a greywacke from the upper slices (plane-polarized light). (b) Chlorite-rich stack partially transformed into mica-chlorite mixed layers (crossed polars). (c,d) Authigenic garnet and vermiculitized biotite (plane-polarized light and crossed polars) from a greywacke of the upper thrust slices.

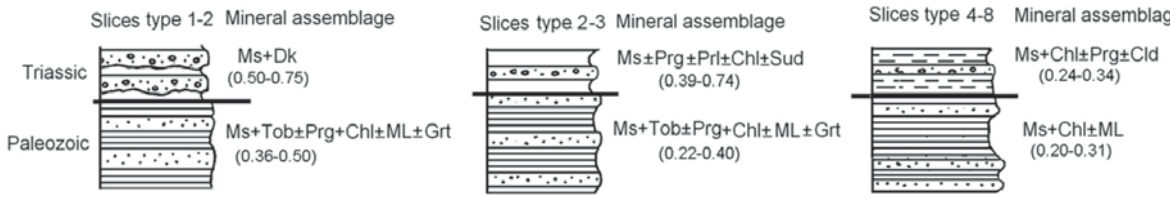

Figure 5. Simplified scheme showing the evolution of the mineral assemblages and the KI range of values (in parentheses) determined in pelitic rocks at the Triassic–Paleozoic transition in each slice, and through the tectonic pile. Mineral symbols according to Kretz (1983) except for Dk: dickite, Tob: tobelite, Sud: sudoite, and ML: mica-chlorite mixed layers. Ms includes muscovite (or phengite) and illite. Symbols in columns as in Figure 2b.

Paleozoic rocks from slices 1–3 show intense reflections of mica (10 Å) and chlorite, together with numerous small reflections, which in some cases are well defined and in other cases occur as shoulders on the chlorite or mica reflections. The clay mineral association consists of white mica + Chl ± ML, which coexist with minor garnet. The apparent KI values (KI values determined before deconvolution) range from 0.36 to 0.50 in slices 1–2 and from 0.22 to 0.40 in slices 2–3. Deconvolution of the mica peaks permitted the identification of several types of mica (Figure 6): K-mica, with the first basal reflection at 10.02 Å; NH_4-mica, with the first reflection at 10.26 Å; and intermediate Na-K-mica, with the first reflection at 9.80 Å. The mean value of the basal spacing of the NH_4-mica, deduced from five basal reflections, was 10.30 Å, indicating that the NH_4-mica present in these rocks must be near the NH_4 end-member (Drits *et al*., 1997). The KI values determined after deconvolution are, as expected, notably lower (in the range 0.24–0.32). From slice 4 the clay mineral association becomes uniform (Ms + Chl ± ML), with KI values between 0.20 and 0.31. Determination of the chlorite crystallinity (Árkai, 1991) is prevented in these samples by the almost continuous presence of mica-chlorite mixed layers, which cause a notable broadening of the 7 Å reflection.

Confirmation of the NH_4-rich nature of the 10.30 Å mica was carried out by IR spectroscopy. A well defined band at 1430 cm^{-1}, ascribed to the N-H vibration (Vedder, 1965; Shigorova *et al*., 1981), was observed in the spectra of the samples containing this phase.

Note that the whole-rock XRD patterns obtained from fine- and coarse-grained rocks indicate that tobelite is more abundant in greywackes than in shales. In addition, the tobelite content does not increase in the fine fractions of the rocks, both facts suggesting that most of the tobelite is probably present in detrital grains.

Two main mineral assemblages, according to the Guidotti and Sassi classification (Guidotti and Sassi, 1976), are present in the Paleozoic samples: assemblage X, with paragonite, white K-mica, and albite; and assemblage Y, with white K-mica and albite. As the *b*-cell method was defined for the Y assemblage, the *b* cell parameters determined have little significance except in paragonite-free, fine-grained samples containing few

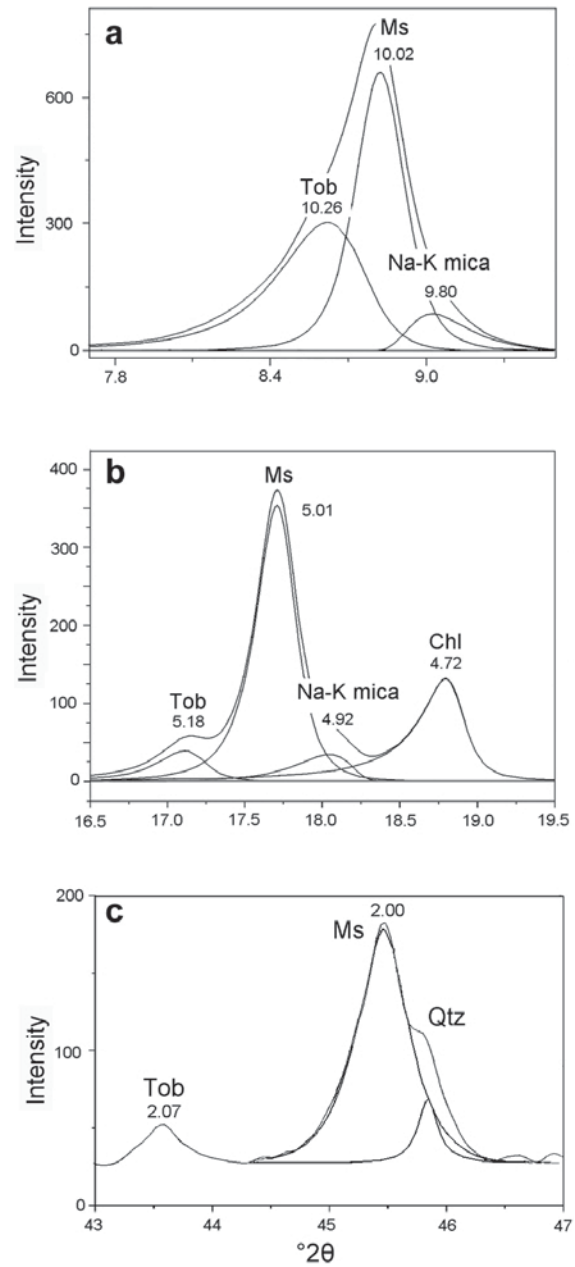

Figure 6. Selected zones of the XRD pattern (oriented sample, <2 μm size fraction) of a tobelite-bearing greywacke. See text for explanation.

detrital constituents. The mean *b* cell parameters for the two mineral assemblages (X and Y) are 9.008 and 9.018 Å, respectively, suggesting a regime of intermediate pressure during mineral crystallization.

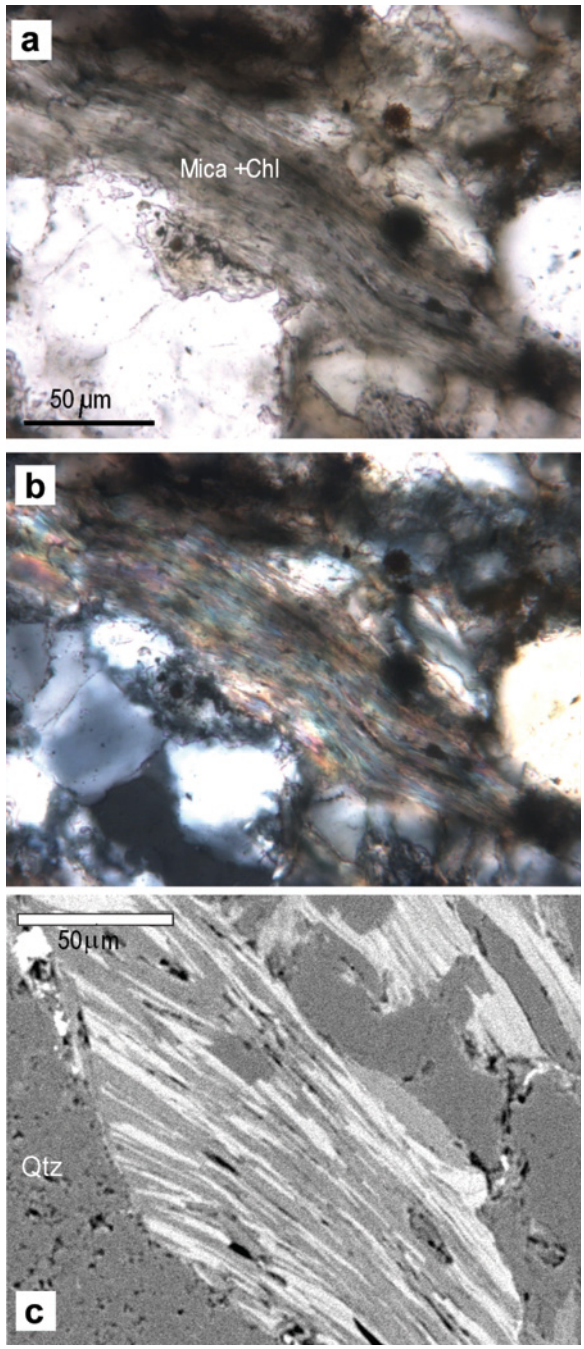

Figure 7. Photomicrographs (a,b) and back-scattered image (c) of 'dirty' mica grains from greywacke of the upper slices. (a) plane-polarized light; (b) crossed nicols.

SEM-EDX data for Paleozoic minerals

White micas. Samples from the upper slices, with the largest apparent tobelite content, were studied extensively by SEM. Two different types of white mica were identified in greywackes from the upper slices on the basis of the optical properties: (1) detrital and authigenic grains of typical colorless mica; (2) detrital 'dirty' mica, with light grey color and slight pleochroism (Figure 7a,b).

The back-scattered images revealed that 'dirty' mica consists of very fine intergrowths of white mica and chlorite (Figure 7c). White mica lamellae show, in addition, small differences in contrast, which correlate with variation in mica Na contents as determined by EDX data (Table 1, analyses 1–7). Representative chemical plots (Figure 8) reveal that, as a whole, white mica lamellae show a phengitic trend (Figure 8a) and

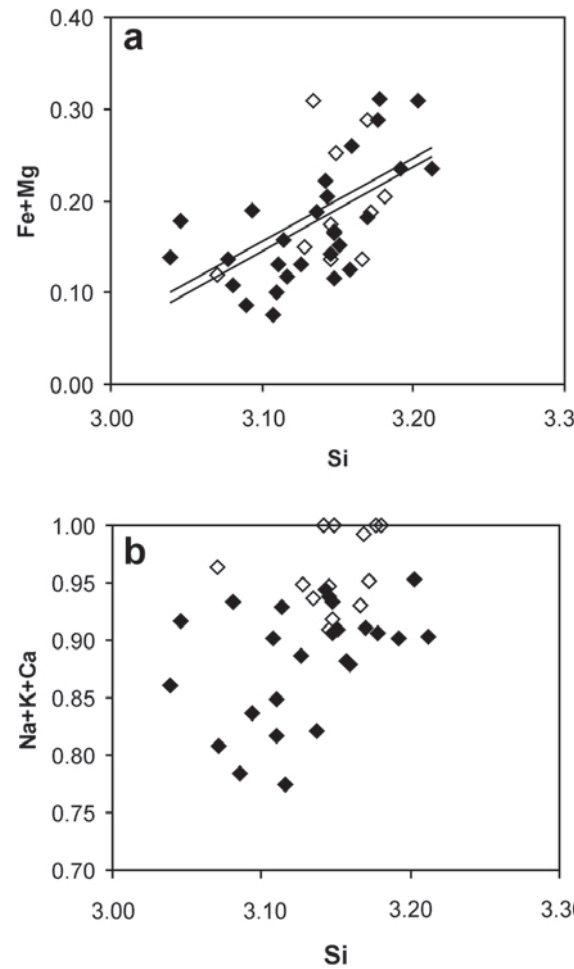

Figure 8. Plots of the more significant chemical characteristics of white micas from the upper slices. (a) Fe+Mg *vs*. Si diagram. (b) Interlayer charge *vs*. Si diagram. Full diamonds: white mica lamellae from 'dirty' mica grains. Open diamonds: clear white mica flakes.

Table 1. EDX and EMPA (*) data for white mica from tobelite-bearing and tobelite-free samples (formulae calculated for $O_{10}(OH)_2$)

	—— Mica lamellae from 'dirty' mica grains (slices 1–3) ——									—— White mica grains from slices 1–3 ——							White mica from slice 5			
	1	2	3	4	5	6	7	Av.	σ	8*	9*	10*	11*	12*	Av.	σ	13	14	Av.	σ
SiO_2	48.55	50.47	49.32	48.97	49.93	49.50	50.74	49.54	0.73	48.62	49.05	48.55	48.65	49.27	48.90	0.28	47.02	49.11	48.23	1.05
Al_2O_3	33.53	35.94	33.53	31.96	33.11	31.75	31.59	33.18	1.40	32.03	32.34	31.17	30.79	30.72	31.77	0.67	31.95	31.94	32.00	0.03
TiO_2	0.21	0.21	0.20	0.41	0.21	0.41	1.24	0.41	0.35	0.20	0.41	0.81	0.40	0.61	0.61	0.21	0.40	0.61	0.40	0.12
FeO	3.17	1.09	1.58	2.78	1.94	2.26	2.13	1.94	0.65	3.31	2.10	1.90	2.93	2.95	2.44	0.55	4.12	1.04	2.60	1.54
MgO	1.19	0.51	0.69	1.07	0.69	0.98	1.09	0.79	0.24	1.17	0.98	1.36	1.26	1.17	1.07	0.13	1.25	1.27	1.26	0.01
CaO	0.14	0.14	0.00	0.00	0.00	0.14	0.00	0.00	0.07	0.14	0.14	0.00	0.13	0.14	0.00	0.07	0.00	0.14	0.00	0.08
Na_2O	2.21	2.66	0.38	0.67	1.14	0.75	1.68	1.60	0.79	0.60	0.38	0.60	0.52	0.45	0.60	0.09	0.82	0.67	0.75	0.07
K_2O	6.25	5.10	9.40	9.19	8.98	9.20	6.88	7.20	1.64	9.91	11.13	10.64	10.59	10.93	10.48	0.42	9.65	9.88	9.74	0.11
Total	95.24	96.12	95.10	95.05	96.01	94.99	95.35	94.66	0.51	95.98	96.53	95.02	95.28	96.24	95.88	0.57	95.22	94.66	94.99	0.28
Si	3.09	3.12	3.15	3.16	3.17	3.19	3.21	3.15	0.05	3.13	3.14	3.15	3.17	3.18	3.15	0.02	3.07	3.17	3.12	0.07
Al^{IV}	0.91	0.88	0.85	0.84	0.83	0.81	0.79	0.85	0.05	0.87	0.86	0.85	0.83	0.82	0.85	0.02	0.93	0.83	0.88	0.09
Al^{VI}	1.77	1.91	1.84	1.75	1.81	1.76	1.72	1.80	0.09	1.72	1.74	1.69	1.69	1.67	1.72	0.05	1.69	1.76	1.72	0.34
Ti	0.01	0.01	0.01	0.02	0.01	0.02	0.06	0.02	0.01	0.01	0.02	0.04	0.02	0.03	0.03	0.01	0.02	0.03	0.02	0.01
Fe	0.18	0.06	0.09	0.16	0.11	0.13	0.12	0.11	0.05	0.19	0.12	0.11	0.17	0.17	0.14	0.04	0.24	0.06	0.15	0.22
Mg	0.12	0.05	0.07	0.11	0.07	0.10	0.11	0.08	0.04	0.12	0.10	0.14	0.13	0.12	0.11	0.02	0.13	0.13	0.13	0.13
Σoct.	2.08	2.04	2.02	2.03	2.00	2.01	2.02	2.02	0.03	2.04	1.98	1.98	2.00	1.99	2.00	0.02	2.09	1.98	2.03	0.03
Ca	0.01	0.01	0.00	0.00	0.00	0.01	0.00	0.00	0.00	0.01	0.01	0.00	0.01	0.01	0.00	0.00	0.00	0.01	0.00	0.00
Na	0.29	0.34	0.05	0.09	0.15	0.10	0.22	0.21	0.16	0.08	0.05	0.08	0.07	0.06	0.08	0.02	0.11	0.09	0.10	0.02
K	0.53	0.42	0.80	0.79	0.76	0.79	0.58	0.61	0.20	0.85	0.95	0.92	0.92	0.94	0.90	0.06	0.84	0.85	0.84	0.10
Σint.	0.84	0.77	0.85	0.88	0.91	0.90	0.80	0.83	0.05	0.94	1.01	1.00	0.99	1.00	0.98	0.04	0.94	0.95	0.96	0.10

very variable interlayer charge (Figure 8b). Some mica lamellae show a dominant potassic composition (Table 1, analyses 3−6). Lamellae or areas with darker contrast show either smaller interlayer charge or greater Na contents or both (Table 1, analyses 1−2). The small interlayer charge of these lamellae (on the order of 0.80 atoms per formula unit − a.p.f.u.) suggests the presence of either some NH_4 content in white K-mica or the presence of NH_4-mica packets submicroscopically intergrown with the Na-K-mica.

Grains of typical white K-mica from slices 1−3 show uniform contrast and more homogeneous compositions, with small Na contents (0.05−0.08 a.p.f.u.) and variable phengitic substitution (Figure 8a). The interlayer charge is generally >0.90 (Table 1, analyses 8−12, Figure 8b), suggesting that the presence of NH_4 is unlikely in this type of mica grain.

White micas from the lower slices show a composition similar to white K-micas from the upper slices (Table 1, analyses 13−14) with small Na content, some phengitic substitution, and interlayer charge on the order of 0.96 a.p.f.u..

Trioctahedral phyllosilicates. Trioctahedral phyllosilicates include chlorite and brownish grains or areas with optical properties like those of vermiculite. Several types of chlorite and brownish grains can be differentiated, especially in the upper slices.

Chlorite lamellae from 'dirty' mica intergrowths (Figure 7c) show Si contents between 2.62 and 2.86 a.p.f.u. (Table 2, analyses 1−3), although some analyses obtained from fine chlorite lamellae are contaminated by the adjacent mica lamellae. Authigenic chlorite and chlorite from detrital chlorite-rich stacks (Figure 9a) show variable Si contents (Table 2, analyses 4−8). The transition from chlorite to the brownish external areas (Figure 4b) is characterized by a notable increase in the Si content and the presence of appreciable amounts of K and minor Na (Table 2, analyses 6−8). The lack of mica lamellae in these areas indicates that the change in composition is not due to contamination but to the presence of mica layers interstratified with chlorite. The increase in Si and K is accompanied by a decrease in octahedral occupancy, suggesting a dioctahedral character for the mica layers interstratified with chlorite. In these grains, textural data as well as the TEM study indicated that these phases consist of regular mica-chlorite mixed layers, and were interpreted to have formed from chlorite during prograde metamorphism (Ruiz Cruz, 2001).

Table 2. Selected EDX and EMPA (*) data for chlorite and 'vermiculite'.

	Chl lamellae from 'dirty' mica grains (upper slices)			Chl partially transformed into mica-chlorite mixed layers (upper slices)					Vermiculitized Bt (upper slices)		Chl and ML from lower slices				
	1	2	3	4*	5(a)*	6(b)*	7(a)*	8(b)*	9	10	11(a)*	12(b)*	13	14	15
SiO_2	28.81	25.56	27.91	26.64	26.98	29.66	30.74	36.37	40.58	40.91	24.35	24.97	24.09	27.72	27.45
TiO_2	1.07	0.06	0.00	0.00	0.74	1.49	2.10	0.08	0.34	0.52	0.05	0.04	0.11	1.16	0.85
Al_2O_3	17.93	22.12	20.97	20.30	18.12	19.59	20.84	23.97	19.80	19.77	22.65	22.80	21.42	22.98	23.24
Cr_2O_3	0.03	0.01	n.d.	n.d.	n.d.	0.09	0.02	0.17	n.d.	n.d.	0.05	0.00	0.03	0.00	0.00
FeO	27.54	26.75	30.86	31.49	33.51	25.76	25.41	21.65	14.39	14.45	31.22	26.52	33.46	29.30	31.77
MnO	0.24	0.47	0.00	0.00	0.00	0.36	0.14	0.16	0.00	0.00	0.17	0.20	0.30	0.85	0.11
MgO	12.56	14.36	8.35	8.56	7.72	9.95	8.51	6.89	5.85	6.85	9.63	6.32	8.83	6.15	5.20
CaO	0.02	0.02	0.00	0.00	0.00	0.15	0.01	0.19	0.00	0.00	0.03	0.08	0.13	0.57	0.25
Na_2O	0.02	0.01	0.00	0.00	0.05	0.04	0.03	0.19	0.00	0.00	0.00	0.01	0.29	0.39	0.51
K_2O	0.01	0.01	0.51	0.00	0.00	1.96	1.16	3.12	4.03	3.89	0.01	0.12	0.27	2.28	2.95
Total	88.28	89.38	88.60	86.99	87.12	89.04	89.95	92.80	84.99	86.39	88.15	81.07	88.88	91.40	92.33
Si	2.62	2.66	2.86	2.78	2.88	3.09	3.16	3.48	3.10	3.08	2.63	2.75	2.64	2.89	2.86
Al^{IV}	1.38	1.34	1.14	1.22	1.12	0.91	0.84	0.52	0.90	0.92	1.37	1.25	1.36	1.11	1.14
Al^{VI}	1.35	1.37	1.56	1.44	1.31	1.49	1.68	2.18	1.00	0.95	1.52	1.71	1.40	1.70	1.71
Ti	0.01	0.00	0.00	0.00	0.06	0.12	0.16	0.01	0.02	0.03	0.00	0.00	0.01	0.09	0.07
Fe	2.52	2.33	2.82	2.93	3.19	2.24	2.18	1.73	0.98	0.97	2.82	2.44	3.07	2.55	2.77
Mn	0.06	0.04	0.00	0.06	0.00	0.03	0.01	0.01	0.00	0.01	0.02	0.02	0.03	0.08	0.01
Mg	2.06	2.23	1.36	1.42	1.31	1.54	1.30	0.98	0.71	0.82	1.55	1.53	1.44	0.96	0.81
Σoct.	6.00	5.97	5.74	5.85	5.87	5.43	5.33	4.92	2.71	2.78	5.91	5.70	5.95	5.38	5.37
Ca	0.00	0.00	0.00	0.00	0.00	0.02	0.00	0.02	0.00	0.00	0.00	0.01	0.01	0.06	0.03
Na	0.00	0.00	0.00	0.00	0.01	0.01	0.01	0.04	0.00	0.00	0.00	0.03	0.06	0.08	0.11
K	0.00	0.00	0.07	0.00	0.00	0.26	0.16	0.38	0.41	0.39	0.00	0.07	0.04	0.30	0.39
Fe/Fe+Mg	0.55	0.51	0.67	0.67	0.71	0.59	0.63	0.64	0.58	0.54	0.64	0.61	0.67	0.73	0.77
O	14	14	14	14	14	14	14	14	11	11	14	14	14	14	14

Analyses (a) and (b) represent, in each sample, the evolution from chlorite areas to mica-chlorite mixed layers.

The detrital 'biotite' flakes show homogeneous contrast and chemical composition (Figure 9b, Table 2: analyses 9–10), both suggesting retrogressive alteration. Alteration leads to an increase in the Si content and a decrease in the interlayer occupancy, as compared with typical biotite, suggesting a process of vermiculitization.

Chlorite from the lower slices shows advanced transformation into mixed-layer phases. The chlorite analyses show Si content on the order of 2.63 a.p.f.u. (Table 2, analysis 11). The transformation is especially evident in phyllites and calc-schists (Figure 9c), where most analyses correspond to chlorite-vermiculite mixed layers (Table 2, analyses 14 and 15).

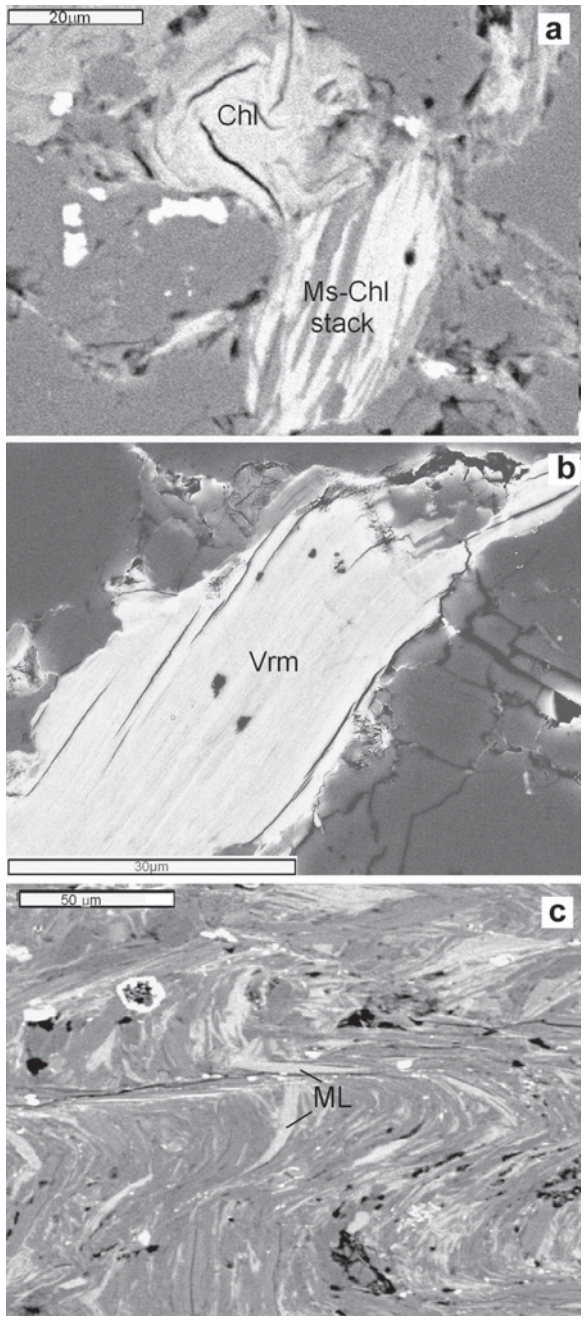

Figure 9. Back-scattered images of the several types of trioctahedral phyllosilicates in Paleozoic rocks. (a) Authigenic chlorite (upper part of the image) and detrital chlorite-rich chlorite-mica stack. (b) Vermiculitized detrital biotite. (c) Laths of mixed layers following S_0 and S_1 in calc-schist from the lower slices.

Garnet. The garnet is compositionally very homogeneous. It is almandine-rich with Ca contents on the order of 0.67 a.p.f.u. (for 12 oxygens), Fe contents on the order of 2.18 a.p.f.u., and Mn contents of <0.05 a.p.f.u. (Table 3).

Transmission electron microscopy study

To identify NH_4-mica in detrital 'dirty' mica grains, some of these grains were selected for study by TEM/AEM. An alternation of sub-parallel, µm-sized mica- and chlorite subgrains can be observed in the TEM images obtained at low magnification (Figure 10). Mica subgrains show a K-rich composition (subgrain 1) or small K contents (subgrain 2), characteristic of tobelite.

Enlarged views (Figure 11) of subgrains 1 and 2 (shown in Figure 10) reveal that subgrains with K-rich composition (Figure 11a) appear formed by parallel or subparallel packets with thickness on the order of 500 Å. Areas with 20 Å periodicity appear only slightly damaged and correspond to K-rich mica, whereas areas with 10 Å periodicity show small K contents (NH_4-rich composition) and deteriorate rapidly, as observed by Nieto (2002).

The subgrains with NH_4-rich composition (Figure 11B) show a greater variation in thickness (from ~100 to >500 Å). The main periodicity measured in the lattice-fringe images and the SAED patterns is near 20.5 Å, although packets showing a ~10 Å periodicity are also common. The SAED patterns obtained (inset in Figure 11) correspond to ordered

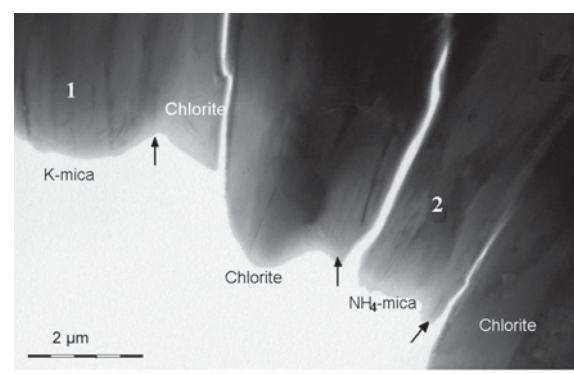

Figure 10. Low-magnification TEM image of a 'dirty' mica grain. Arrows indicate the approximate position of the boundary between subgrains with different compositions.

Table 3. Selected EMPA data for garnets (formulae calculated for 12 O).

	1	2	3
SiO_2	37.39	36.79	37.86
Al_2O_3	21.19	21.17	21.27
TiO_2	0.08	0.08	0.08
FeO	32.95	32.58	33.13
MnO	0.37	0.35	0.38
MgO	1.54	1.63	1.83
NiO	0.00	0.01	0.01
Cr_2O_3	0.00	0.02	0.01
CaO	8.01	7.83	7.64
Na_2O	0.03	0.04	0.66
K_2O	0.00	0.01	0.03
Total	101.55	100.51	101.89
Formulae			
Si	2.96	2.94	2.95
Al	1.98	2.00	1.94
Ti	0.00	0.00	0.00
Fe	2.18	2.18	2.16
Mn	0.02	0.02	0.02
Mg	0.18	0.19	0.21
Ca	0.68	0.67	0.64
Na	0.00	0.00	0.10

two-layer polytypes ($2M_1$) in both K- and NH_4-rich packets. Splitting of the 00*l* reflections was not generally observed in the SAED patterns obtained from K- and NH_4-rich packets, suggesting that finer intergrowths of K- and NH_4-mica are lacking.

EDX spectra (Figure 11, inset) show that K-rich mica packets have a rather uniform composition in the several subgrains analyzed, with small Fe and Mg contents. The tobelite packets show a more variable composition, with greater celadonite substitution. The EDX spectra of these packets showed the sporadic presence of N (Figure 11, inset c), although this element disappeared from the spectra after 2−3 s. Large Na contents characterize some NH_4-rich packets in such a way that these areas contain similar amounts of Na and K.

DISCUSSION

Evolution of micas at increasing tectonic grade

The Triassic sequences of the intermediate units show a clear evolution of mineral assemblages at increasing tectonic grade: Ms + Dk, Ms + Prl + Sud, and Ms + Chl + Prg + Cld (Figure 5), in addition to quartz, minor feldspar, and Fe oxide. In parallel, the composition of white micas indicates a transition from illite (in the upper slices) to muscovite with important Na contents in the lower chloritoid-bearing rocks (Ruiz Cruz *et al*., 2005).

The Paleozoic rocks, in contrast, show a rather homogeneous mineralogical composition through the tectonic sequence, consisting of Qtz + Ab ± Cal + Ms ± Prg ± Tob + Chl ± ML, where only the composition of the micas can be correlated with the tectonic grade (*i.e*. with the Maláguide- or Alpujárride-like character of the slices). The upper thrust slices are characterized by the presence of tobelite and Na-bearing micas (paragonite and intermediate Na-K mica). At increasing tectonic grade, the NH_4-micas and, later, the Na-bearing micas, gradually disappear. The study by TEM confirmed that NH_4-mica (and some of the Na-K mica) from the upper slices is present in detrital micaceous minerals, in contrast with previous tobelite descriptions from Paleozoic rocks, where it occurs in illitic mineral structures (*e.g.* Juster *et al*., 1987; Daniels and Altaner, 1990; Nieto, 2002). Nevertheless, the presence of some illitic tobelite in the rock matrix cannot be excluded based on the available data.

Mineral genesis

In contrast to Triassic sequences, which were only affected by the Alpine metamorphism, two metamorphic episodes (Hercynian and Alpine) have been identified in typical Maláguide Paleozoic sequences. The presence of a pre-Alpine metamorphic event in the Maláguide Paleozoic was hypothesized by Felder (1980) on the basis of the rapid change in the size of the mica and chlorite at the Triassic to Paleozoic transition. The increase in size of the white mica was accompanied by a decrease in KI, which varied from low to high anchizonal values (Ruiz Cruz and Rodríguez Jiménez, 2002). In addition, the rapid decrease of the Si content of chlorite revealed a temperature gap of ~150ºC in Triassic rocks to ~300ºC in Paleozoic samples (Ruiz Cruz, 1997).

The evolution of the mineral assemblages at the transition from Triassic to Paleozoic rock sequences and at increasing tectonic grade in the intermediate units (Figure 5) reveals that both mineral assemblages and KI values show, as in typical Maláguide sequences, a clear discontinuity between Triassic and Paleozoic rocks, especially evident in the upper thrust slices. Changes in clay mineral associations can be related to differences in bulk-rock composition. Nevertheless, the important decrease in the KI values at the transition from Triassic to Paleozoic units (upper thrust slices) reveals a rapid increase in metamorphic temperature, which can be only explained if the KI values of the upper Paleozoic slices correspond to Hercynian micas. A notable discontinuity in metamorphic temperatures between Triassic and Paleozoic rocks can also be deduced from the change of dickite-bearing assemblages, characteristic of the Triassic rocks (with estimated temperatures of ~150ºC), to the garnet-bearing assemblages of Paleozoic rocks. Estimation of the temperature of the Paleozoic assemblage has been carried out tentatively using the muscovite-garnet geothermometer, used for different calibrations (Krogh and Rahein, 1978; Hynes and Forest, 1988) and different garnet solution models (ideal mixing: Hodges and Spear, 1982; Ganguly and

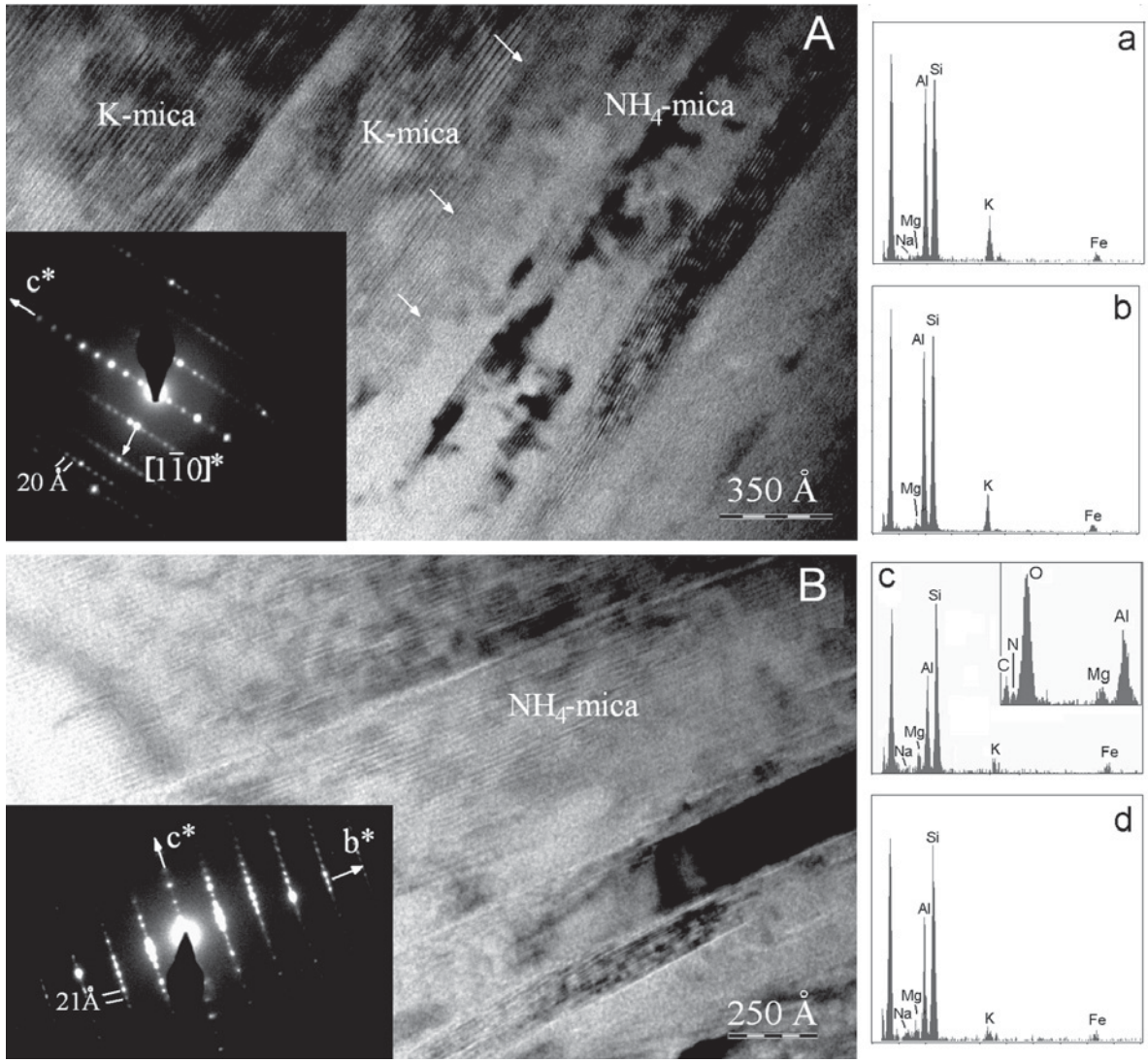

Figure 11. (A) Lattice-fringe image of an area of subgrain 1 (Figure 10) made up of subparallel packets of K-mica and NH_4-mica. K-mica packets show a 20 Å periodicity whereas damaged NH_4-mica packets show a ~10.5 Å periodicity. The SAED pattern (inset) shows the two-layer periodicity characteristic of the $2M_1$ polytype. Arrows mark the approximate boundary between the K- and NH_4-rich areas. (B) Lattice-fringe image of a selected area of subgrain 2 (Figure 10), showing the ~21 Å periodicity of the NH_4-mica packets, as also shown by the SAED pattern (inset). (a,b) EDX spectra of K-rich packets. (c,d) EDX spectra of NH_4-rich packets.

Saxena, 1984; Hoinkes, 1986). This geothermometer provides temperatures between 400ºC and 460ºC which means that most fine-grained white K-mica and garnet from the upper slices grew during the Hercynian event.

In the lower slices, the metamorphic gap between Triassic and Paleozoic rocks is less evident. Indeed, the KI values are in the ranges 0.20−0.31 and 0.24−0.34 for Paleozoic and Triassic rocks, respectively. Moreover, using the chloritoid-chlorite thermometer (Vidal *et al*., 1999), Ruiz Cruz *et al*. (2005) deduced maximum temperatures of 412 ± 20ºC for the Triassic chloritoid-bearing parageneses. These data suggest that the mineral evolution observed in Triassic sequences at the transition from Maláguide to Alpujárride was mainly controlled by increasing temperatures related to the Alpine event. In contrast, the homogeneous mineral assemblages observed in upper Paleozoic sequences suggest that the metamorphic conditions of the Hercynian event were rather uniform in the transitional units.

The interpretation of two of the phases identified in Paleozoic rocks (tobelite and mica-chlorite mixed layers) is more problematic. The SEM and TEM data indicate that tobelite is finely intergrown with white mica in grains with a detrital provenance, whereas other mica grains from the host rock appear to be NH_4 free. This indicates that tobelite was derived from a detrital NH_4-rich

precursor. Tobelite has been identified only in the upper thrust slices, suggesting that changes in the supplies are the principal factors responsible for the disappearance of tobelite at the transition from the Maláguide to the Alpujárride domain. Whether tobelite was already present in the detrital grains or grew during a retrogressive event from precursor NH_4-bearing mica is uncertain based on the available data. Taking into account the composition of the two intergrown micas (K- and NH_4-rich) near the pure end members (Figure 11, inset), their origin is probably related to low-temperature processes.

Although vermiculitized grains of detrital biotite (Figure 4c) have a clear retrogressive character, the mica-chlorite mixed layers formed from chlorite transformation (Figures 3d, 4b) and are interpreted as prograde phases, following Maresch *et al.* (1985), Ruiz Cruz (2001), and Ruiz Cruz and Nieto (2006). A similar transformation of chlorite has yet to be observed in the Triassic rocks, suggesting that mixed layers also formed during the Hercynian metamorphic event.

CONCLUSIONS

Tobelite has been identified for the first time in upper Paleozoic rocks from units intermediate between the Maláguide and Alpujárride complexes. In contrast with previous tobelite descriptions in Paleozoic rocks, where it has an authigenic origin, the SEM and TEM observations indicate that tobelite is present in detrital grains, consisting of fine intergrowths of muscovite, tobelite, and chlorite. Although the mica + chlorite intergrowths are detrital in origin, the muscovite + tobelite intergrowths probably formed at low temperature from precursor detrital NH_4-bearing mica.

The metamorphic gap observed in both mineral assemblages and KI values between Paleozoic and Triassic sequences from the same tectonic slices (upper slices) reveal a rapid temperature increase, which can only be explained if the Paleozoic micas formed during the Hercynian episode. The Alpine event, which is clearly reflected in the change in mineral assemblages and KI values of Triassic rocks, at increasing tectonic grades (and increasing temperatures), scarcely affected the Paleozoic rocks from the upper tectonic slices where Hercynian phases were preserved.

The evolution from Maláguide- to Alpujárride-like Paleozoic units, at increasing tectonic grades is mainly marked in the sequences studied by a gap in mineral assemblages between slices 2 and 3 (Diezma section) and 3 and 4 (El Molinillo section). This gap is due to a change in the detrital supplies (presence and absence of detrital tobelite-bearing grains) at the transition from Maláguide- to Alpujárride-like thrust slices, revealing a clear transition in paleogeographic position between both complexes. Uniformity in mineral associations (excluding the presence of tobelite) and in KI values, when these are calculated after deconvolution of the mica peak (beginning of the epizone), suggest that the Paleozoic sequences were affected during the Hercynian episode by uniform metamorphic conditions (~400ºC and intermediate pressures).

ACKNOWLEDGMENTS

The authors are grateful to J.W. Stucki, H. Dong, and two unknown reviewers for the careful reviews of the manuscript; to M.M. Abad (Universidad de Granada) for help in obtaining TEM/AEM data; and to M. Bentabol for the FTIR spectra. This study received financial support from Project CGL 2009-08186 (Ministerio de Ciencia e Innovación) and from Research Group RNM-199 (Junta de Andalucía).

REFERENCES

Árkai, P. (1991) Chlorite crystallinity: an empirical approach and correlation with illite crystallinity, coal rank and mineral facies as exemplified by Palaeozoic and Mesozoic rocks of northeast Hungary. *Journal of Metamorphic Geology*, **9**, 723–734.

Árkai, P., Merriman, R.J., Roberts, B., Peacor, D.R., and Tóth, M. (1996) Crystallinity, crystallite size and lattice strain of illite-muscovite and chlorite: comparison of XRD and TEM data for diagenetic and epizonal pelites. *European Journal of Mineralogy*, **8**, 1119–1137.

Árkai, P., Livi, K.J.T., Frey, M., Brukner-Wein, A., and Sajgó, C. (2004) White micas with mixed interlayer occupancy: a possible cause of pitfalls in applying illite Kübler index ("crystallinity") for the determination of metamorphic grade. *European Journal of Mineralogy*, **16**, 469–482.

Azañón, J.M., García-Dueñas, V., and Goffé, B. (1998) Exhumation of high-pressure metapelites and coeval crustal extension in the Alpujárride complex. *Tectonophysics*, **285**, 231–252.

Bobos, I. and Ghegari, L. (1999) Conversion of smectite to ammonium illite in the hydrothermal system of Harghita Bai, Romania: SEM and TEM investigations. *Geologica Carpathica*, **50**, 319–333.

Booth-Rea G., Azañón, J.M., Goffé, B., Vidal, O., and Martínez-Martínez, J.M. (2002) High-pressure, low-temperature metamorphism in Alpujárride Units of southeastern Betics (Spain). *Comptes Rendues, Geosciences*, **334-11**, 857–865.

Cliff, G. and Lorimer, G.W. (1975) The quantitative analysis of thin specimen. *Journal of Microscopy*, **103**, 203–207.

Daniels, E.J. and Altaner, S.P. (1990) Clay mineral authigenesis in coal and shale from the Anthracite region, Pennsylvania. *American Mineralogist*, **75**, 825–839.

Drits, V.A., Lindgreen, H., and Salyn, A.L. (1997) Determination of the content and distribution of fixed ammonium in Illite-smectite by X-ray diffraction: Application to North See Illite-smectite. *American Mineralogist*, **82**, 79–87.

Egeler, C.G. and Simon, O.J. (1969) Orogenic evolution of the Betic Zone (Betic Cordilleras, Spain), with emphasis on the nappe structures. *Geologie en Mijnbouw*, **48**, 296–305.

Felder, T.E. (1980) Geologic evolution of the westernmost part of the Internal Betic Zone (Betic Cordilleras, Southern Spain). *Geologische Rundschau*, **69**, 131–148.

Frey, M. (1987) Very low-grade metamorphism of clastic sedimentary rocks. In: *Low Temperature Metamorphism* (M. Frey, editor). Blackie and Sons Ltd, Glasgow, UK.

Ganguly, J. and Saxena, S.K. (1984) Mixing properties of aluminosilicate garnets: constraints from natural and experimental data, and applications to geothermobarometry.

American Mineralogist, **69**, 88–97.

Goffé, B., Michard, A., García-Dueñas, V., González-Lodeiro, F., Monié, P., Campos, J., Galindo-Zaldívar, J., Jabaloy, A., Martínez-Martínez, J.M., and Simancas, F. (1989) First evidence of high-pressure, low temperature metamorphism in the Alpujarride nappes, Betic Cordillera (SE Spain). *European Journal of Mineralogy*, **1**, 139–142.

Guidotti, C.V. and Sassi, F.P. (1976) Muscovite as a petrogenetic indicator mineral in pelitic schist. *Neues Jahrbuch für Mineralogie Abhandlungen*, **127**, 97–142.

Higashi, S. (1982) Tobelite, a new ammonium dioctahedral mica. *Mineralogical Journal*, **11**, 138–146.

Hodges, K.V. and Spear, F.S. (1982) Geothermometry, geobarometry and the Al_2SiO_5 triple point at Mt. Moosilauke, New Hampshire. *American Mineralogist*, **67**, 1118–1134.

Hoinkes, G. (1986) Effect of grossular content in garnet on the partitioning of Fe and Mg between garnet and biotite. *Contributions to Mineralogy and Petrology*, **92**, 393–399.

Hynes, A. and Forest, R.C. (1988) Empirical garnet-muscovite geothermometry in low-grade metapelites, Selwyn Range (Canadian Rockies). *Journal of Metamorphic Geology*, **6**, 297–309.

Juster, T.C., Brown, P.E., and Bailey, S.W. (1987) NH_4-bearing illite in very low grade metamorphic rocks associated with coal, northeastern Pennsylvania. *American Mineralogist*, **72**, 555–565.

Kisch, H.J. (1991) Illite crystallinity; recommendations on sample preparation, X-ray diffraction settings, and interlaboratory samples. *Journal of Metamorphic Geology*, **9**, 665–670.

Kretz, R. (1983) Symbols for rock-forming minerals. *American Mineralogist*, **68**, 277–279.

Krogh, E.J. and Rahein, A. (1978) Temperature and pressure dependence of Fe-Mg partitioning between garnet and phengite, with particular reference to eclogites. *Contributions to Mineralogy and Petrology*, **66**, 75–80.

Kübler, B. (1968) Evaluation quantitative du métamorphisme par la cristallinité de l'illite. Etat des progrès réalisés ces dernières années. *Bulletin Centre Recherche Pau, S.N.P.A.*, **2**, 385–397.

Liu, Q., Zhang, P., Dings, S., Lin, X., and Zheng, N. (1996) NH_4-illite in Permo-Carboniferous coal-bearing strata, North China. *Chinese Science Bulletin*, **41**, 1458–1461.

Mäkel, G.H. (1985) The geology of the Maláguide complex and its bearing on the geodynamic evolution of the Betic-Rif orogen (Southern Spain and Northern Morocco). *GUA Papers of Geology*, **22**. 263 pp.

Mäkel, G.H. and Rondeel, H.E. (1979) Differences in stratigraphy and metamorphism between superposed Maláguide and Alpujárride units in the Espuña area (Betic Cordilleras, Spain). *Estudios Geológicos*, **35**, 109–117.

Maresch, W.V., Massone, H.-J., and Czank, M. (1985) Ordered and disordered chlorite/biotite interstratifications as alteration products of chlorite. *Neues Jahrbuch für Mineralogie Abhadlungen*, **152**, 79–100.

Merriman, R.J. and Peacor, D.R. (1999) Very low-grade metapelites: mineralogy, microfabrics and measuring reaction progress. Pp. 10–60 in: *Low-grade Metamorphism* (M. Frey and D. Robinson, editors). Blackwell Science, Oxford, UK.

Merriman, R.J., Roberts, B., and Peacor, D.R. (1990) A transmission electron microscope study of white mica crystallite size distribution in a mudstone to slate transitional sequence, North Wales, U.K. *Contributions to Mineralogy and Petrology*, **106**, 27–40.

Merriman, R.J., Roberts, B., Peacor, D.R., and Hirons, S.R. (1995) Strain-related differences in the crystal growth of white mica and chlorite: a TEM and XRD study of the development of metapelite microfabrics in the Southern Uplands thrust terrane, Scotland. *Journal of Metamorphic Geology*, **13**, 559–576.

Nieto, F. (2002) Characterization of coexisting NH_4- and K-micas in very low-grade metapelites. *American Mineralogist*, **87**, 205–216.

Paquet, J. (1969) Étude géologique de l'Ouest de la province de Murcie. *Bulletin de la Societé géologique de France*, **111**, 1–270.

Ruiz Cruz, M.D. (1997) Very low-grade chlorite with anomalous chemistry and optical properties from the Maláguide Complex, Betic Cordilleras, Spain. *The Canadian Mineralogist*, **35**, 923–935.

Ruiz Cruz, M.D. (2001) Mixed-layer mica-chlorite in very low-grade metaclastites from the Maláguide Complex (Betic Cordilleras, Spain). *Clay Minerals*, **36**, 307–324.

Ruiz Cruz, M.D. and Rodríguez Jiménez, P. (2002) Correlation between crystallochemical parameters of phyllosilicates and mineral facies in very low-grade metasediments of the Betic Cordillera (Spain): A synthesis. *Clay Minerals*, **37**, 169–185.

Ruiz Cruz, M.D. and Nieto, J.M. (2006) Chemical and structural evolution of "metamorphic vermiculite" in metaclastic rocks of the Betic Cordillera, Málaga, Spain: A synthesis. *The Canadian Mineralogist*, **44**, 249–265.

Ruiz Cruz, M.D., Sanz de Galdeano, C., and Lázaro, C. (2005) Metamorphic evolution of Triassic rocks from the transition zone between the Maláguide and the Alpujárride complexes (Betic Cordilleras, Spain). *European Journal of Mineralogy*, **17**, 81–91.

Sanz de Galdeano, C., Andreo, B., García-Tortosa, F.J., and López-Garrido, A.C. (2001) The Triassic palaeogeographic transition between the Alpujárride and Maláguide complexes. Betic-Rif Internal Zone. *Palaeo*, **167**, 157–173.

Shigorova, T.A., Kotov, N.V., Kotelnikova, Ye.N., Shamakin, B.M., and Frank-Kamenetski, V.A. (1981) Synthesis, diffractometry and IR spectroscopy of micas in the series from muscovite to the ammonium analog. *Geochemistry International*, **18**, 76–82.

Vedder, W. (1965) Ammonium in muscovite. *Geochimica et Cosmochimica Acta*, **29**, 221–228.

Velde, B. (1978) High temperature or metamorphic vermiculites. *Contributions to Mineralogy and Petrology*, **66**, 319–323.

Vidal, O., Goffé, B., Bousquet, R., and Parra, T. (1999) Calibration and testing of an empirical chloritoid-chlorite Mg-Fe exchange thermometer and thermodynamic data for daphnite. *Journal of Metamorphic Geology*, **17**, 25–39.

Ward, C.R. and Christie, P.J. (1994) Clays and other minerals in coal seams of the Moura-Baralaba area, Bowen Basin, Australia. *International Journal of Coal Geology*, **25**, 287–309.

Warr, L.C. and Rice, H.N. (1994) Interlaboratory standarization and calibration of clay minerals crystallinity and crystallite size data. *Journal of Metamorphic Geology*, **12**, 141–152.

Wilson, P.N., Parry, W.T., and Nash, W.P. (1992) Characterization of hydrothermal tobelitic veins from black shales, Oquirrthe Mountains, Utah. *Clays and Clay Minerals*, **40**, 405–420.

Zeck, H.P. and Whitehouse, M.J. (1999) Hercynian, Pan-African, Proterozoic and Archean ion-microprobe zircon ages for a Betic-Rif core complex, Alpine belt, W Mediterranean – consequences for its P-T-t path. *Contributions to Mineralogy and Petro*logy, **134**, 134–149.

(*Received 18 November 2009; revised 29 June 2010; Ms. 375; A.E. H. Dong*)